Supplementary Information

Oxygen Dynamics in Intertidal Sediments: Integrating High-Resolution Data and Reaction-Transport Modeling

Qi Liu, Karline Soetaert, Lucille Hoogerdijk, Valle Perez Rodriguez, Lubos Polerecky

Supplementary Methods

Technical details of the experimental setup

Laboratory experiments were conducted in sediment cores placed in a transparent glass aquarium (dimensions: 50 cm × 35 cm × 42 cm) filled with seawater (Figure **S1**). Water level in the aquarium was adjusted using a tube connected to a pump, while water temperature was controlled using a heater/chiller circulator (Lauda Ecoline RE 206). A fiber-optic light source (KL 1600, Schott) equipped with a halogen lamp and a near-infrared (NIR) filter provided stable but adjustable illumination of the sediment surface with a spectrum similar to that of solar radiation. Incident irradiance at the sediment surface was determined using a calibrated light meter (LI-250A, LI-COR).

To achieve a stable diffusive boundary layer (DBL) above the sediment surface, a continuous air stream was directed across the water surface in the core through a fine micro-pipette connected to an air pump, generating a gentle unidirectional flow in the overlying water that produced laminar flow conditions near the sediment-water interface (SWI). To keep the overlying water air-saturated throughout the measurements, a porous stone connected to an air pump was used to gently bubble air through the overlying water. The stone was placed at a sufficient distance from the SWI to minimize DBL disturbance by the bubbling.

O_2 concentrations were measured using a fast-response Clark-type O_2 microelectrode (OX-50) connected to a multimeter equipped with an analog-to-digital converter (both purchased from Unisense A/S). The microelectrode had a tip diameter of ∼50 µm and response time of $t_{90} \approx 0.5$ s. Vertical light distributions in the sediment were measured with a fiber-optic scalar irradiance microprobe (supplied by Lars Rickelt, Zenzor) connected to a spectrometer (USB2000+, Ocean Optics). The microprobe had a spherical tip (diameter of ∼80 µm) attached to a tapered optical fiber (diameter of 100 µm). During measurements, the O_2 or light microsensor was mounted on a 3-axis manual micromanipulator attached to a motorized linear positioner (Unisense A/S, Denmark), which allowed reproducible positioning of the sensor tip with a precision of about 2 µm. Precise alignment of the microsensor tip at the SWI was aided by a stereomicroscope (M80, Leica Microsystems).

Measurements were automated using a laptop. The software package OceanView (Ocean Optics) was used to acquire the light spectra, whereas Profiler (Unisense A/S) was used to control the linear positioner and signal acquisition from the O_2 microsensor.

Boundary conditions in the model

For O_2, the model uses a fixed concentration at the upper boundary. This concentration is expressed as a product

$$C_{O_2}|_{z=-z_{\mathrm{DBL}}} = \alpha_{O_2} \cdot C_{O_2}^{max}, \tag{1}$$

where α_{O_2} is the relative saturation (typically a value ≤ 1) and $C_{O_2}^{max}$ is the air-saturated concentration of dissolved O_2. The latter value is calculated according to Henry's law,

$$C_{O_2}^{max} = S_{O_2}(T, S) \cdot P_{O_2}, \tag{2}$$

where $S_{O_2}(T, S)$ (in $\mathrm{mol\,O_2/m^3/atm}$) is the temperature ($T$) and salinity ($S$) dependent O_2 solubility in seawater, computed with the R package `marelac`, and $P_{O_2} \approx 0.2095\,\mathrm{atm}$ is the atmospheric partial pressure of O_2. The same expressions are used when the sediment surface is submerged or exposed to air. A zero-gradient condition is assumed for the lower boundary, i.e.,

$$\left.\frac{\partial C_{O_2}}{\partial z}\right|_{z=z_{\mathrm{sed}}} = 0, \tag{3}$$

which corresponds to no diffusive O_2 flux at the bottom of the sediment column.

For ODU, the model assumes zero concentration at the upper boundary,

$$C_{\mathrm{ODU}}|_{z=-z_{\mathrm{DBL}}} = 0, \tag{4}$$

which represents immediate ODU reoxidation above the DBL if O_2 is present. For the lower boundary, a fixed concentration is assumed, i.e.,

$$C_{\mathrm{ODU}}|_{z=z_{\mathrm{sed}}} = C_{\mathrm{ODU}}^{\mathrm{deep}}, \tag{5}$$

where $C_{\mathrm{ODU}}^{\mathrm{deep}}$ (in $\mathrm{mol\,O_2/m^3}$) is constrained by matching the model output to the measured O_2 concentration profiles. This condition reflects the concept that, with respect to biogeochemical O_2 consumption via ODU reoxidation, the deeper sediment acts as an infinite reservoir of reduced species produced continuously by anaerobic mineralization. For simplicity, this value is assumed to be temperature independent.

Once the model is solved using the boundary conditions listed above, it outputs the corresponding diffusive fluxes across the upper and lower boundaries, calculated from the concentration gradients and Fick's first law of diffusion. Specifically, the diffusive flux of O_2 at the SWI is calculated according to

$$J_{O_2}^{\mathrm{SWI}} = -D_{O_2} \cdot \left.\frac{\partial C_{O_2}}{\partial z}\right|_{z=0}, \tag{6}$$

whereas the flux at the lower boundary is equal to zero,

$$J_{O_2}^{\mathrm{deep}} = 0, \tag{7}$$

in line with the lower boundary condition (Eq. 3). Analogously, the diffusive flux of ODU is calculated according to

$$J_{\mathrm{ODU}}^{\mathrm{SWI}} = -D_{\mathrm{ODU}} \cdot \left.\frac{\partial C_{\mathrm{ODU}}}{\partial z}\right|_{z=0} \tag{8}$$

for the SWI and

$$J_{\mathrm{ODU}}^{\mathrm{deep}} = -D_{\mathrm{ODU}} \cdot \left.\frac{\partial C_{\mathrm{ODU}}}{\partial z}\right|_{z=z_{\mathrm{sed}}} \tag{9}$$

for the lower boundary.

Typical steps used during model calibration

The following steps were employed to constrain the model parameters based on the experimental data acquired in the present study.

The first step involved fitting the vertical profile of GPP (O_2 production) rates, achieved by adjusting the parameters controlling the MPB biomass (C_{MPB}), its vertical distribution (μ and σ), and productivity ($r_{photosyn}$). Although chlorophyll *a* measurements were used to estimate the total MPB biomass in the sampled sediments, their substantial inter- and intra-core variability precluded their direct use as a strict constraint. Instead, they provided an order-of-magnitude reference for the parameter C_{MPB}. Therefore, the rate coefficient $r_{photosyn}$ was first constrained based on literature-reported values, followed by the adjustment of C_{MPB} to match the magnitude of the measured GPP rates. Subsequently, parameters μ and σ were tuned to reproduce the observed shape of the GPP profile. This approach ensured that the estimated parameters remained within a realistic range while accounting for the high variability in the observational data.

After fitting the profile of GPP rates, the next step involved fitting the steady-state vertical profiles of O_2 concentrations. This was achieved by adjusting the parameters controlling O_2 consumption, including $r_{basalresp}$, r_{reox}, $c_{aeromin}$, and $c_{photoresp}$. Among them, $r_{basalresp}$ was constrained first, using O_2 profiles measured under dark conditions. Then, using O_2 profiles measured at low to moderate levels of incident irradiance, $c_{aeromin}$ was constrained mainly based on the magnitude of the O_2 peak, while r_{reox} was constrained based on the O_2 penetration depth. Finally, O_2 profiles measured at the highest levels of incident irradiance, where O_2 concentrations reached extremely high values, were used to constrain $c_{photoresp}$.

This step-wise approach was followed for each GPP and O_2 profile acquired under different experimental conditions, using visual inspection and parameter consistency across a particular experiment as the main quality control criteria. First, data acquired during the PI experiment were used to constrain the parameters controlling the light response (k_I and w) of the studied MPB community. These values were subsequently inherited when constraining the parameters controlling the response to temperature (T_{max}, T_{min} and T_{opt} for each process) and emersion (g_0) using data from the TR and IE experiments, respectively.

Supplementary Tables

Table S1: Conditions during the three types of experiments conducted in the present study. The sampling times of the sediment cores are also included.

Replicate	**Incident irradiance** (µmol photons/m^2/s)	**Temperature** (°C)	**Water height** (m)	**Sampling time**
photosynthesis-irradiance (PI) experiment				
core 1	50, 100, 200, 400, 800	23	0.02	September 2023
core 2	90, 170, 250, 370, 540, 730	23	0.02	September 2023
core 3	90, 170, 265, 350, 540, 730	23	0.02	September 2023
temperature-ramping (TR) experiment				
core 4	170	14, 20.7, 25.7, 29.6, 34.6, 40.2	0.02	September 2023
core 5	320	14.8, 26.1, 35.2, 45.3	0.02	October 2023
core 6	150	16, 25.2, 35.3, 40, **16**	0.02	October 2023
immersion-emersion (IE) experiment				
core 7	150	15	0.02, 0	November 2023
core 8	209	11.8	0.02, 0	March 2024
core 9	230	10	0.02, 0	March 2024

Table S2: MPB biomass derived from Chlorophyll-a measurements. Data for replicate cores 2 and 3 from the PI experiment and for all cores in the IE experiment are not available.

Core	Replicate	Sample weight (g)	Chl-a (µg g^{-1} dw)	MPB biomass† (mol C/m^2)	Core average (mol C/m^2)
Photosynthesis-irradiance (PI) experiment					
Core 1	A	0.39	628.53	20.43	27.38
	B	0.54	745.60	33.55	
	C	0.55	614.41	28.16	
Temperature ramping (TR) experiment					
Core 4	A	2.21	189.15	34.84	27.10
	B	2.11	97.28	17.11	
	C	1.91	184.41	29.35	
Core 5	A	2.10	168.74	29.53	27.23
	B	2.03	135.94	23.00	
	C	1.20	291.57	29.16	
Core 6	A	0.11	346.45	3.18	4.20
	B	0.14	369.98	4.32	
	C	0.16	382.93	5.11	

†Chlorophyll-a concentrations (in µg Chl-a per g of dry sediment) were converted to areal MPB biomass (in mol C/m^2) based on the area of the sampled sediment (1 cm^2), molar weight of C (12 g mol^{-1}), and assuming a carbon-to-chlorophyll-a ratio of 100 g C/g Chl-a.

Table S3: List of model parameters. (Continues on the next page.)

Parameter	Default Value	Unit	Description	Source
Sediment				
z_{DBL}	0.0002	m	Thickness of the diffusive boundary layer	2
z_{sed}	0.005	m	Thickness of the sediment layer	2
θ	0.9	$\mathrm{m}^3_{\mathrm{liquid}}/\mathrm{m}^3$	Volumetric porosity	2
Environment				
α_{O_2}	1	–	Relative air saturation of water at the upper boundary	2
T	23	°C	Temperature of the system	2
S	31	–	Salinity of seawater	2
$C^{\mathrm{deep}}_{\mathrm{ODU}}$	13	$\mathrm{mol}/\mathrm{m}^3_{\mathrm{liquid}}$	ODU concentration at the lower boundary	3
$k_{\mathrm{ext,liquid}}$	1	m^{-1}	Light extinction coefficient of sediment porewater	3
$k_{\mathrm{ext,solid}}$	10^5	m^{-1}	Light extinction coefficient of sediment solids	3
MPB				
B_{MPB}	24	$\mathrm{mol\,C}/\mathrm{m}^2$	MPB biomass per unit area	3
k_I	200	$\mathrm{\mu mol\,photons}/\mathrm{m}^2/\mathrm{s}$	Optimal light intensity for MPB photosynthesis	3, 1^a
w	10	–	Parameter controling the shape of the light response curve	3, 1^a
μ	0.39×10^{-3}	m	Depth of the maximum MPB biomass	3
σ	Eq. 15	m	Dispersion of the MPB biomass distribution	3
Process rates				
$r_{photosyn}$	0.15	d^{-1}	Rate coefficient of MPB photosynthesis at T	3
$r_{basalresp}$	0.0002	d^{-1}	Rate coefficient of MPB basal (dark) respiration at T	3
r_{reox}	5000	d^{-1}	Rate coefficient of ODU reoxidation at T	3
$c_{aeromin}$	0.38	–	Fraction of photosynthetically produced O_2 removed by aerobic mineralization	3
$c_{photoresp}$	0.001	–	Fraction of photosynthetically produced O_2 removed by photorespiration	3
m	4	–	Reaction order of photorespiration	3, 1^b
g_0	0.4	–	Fraction of MPB photosynthesis in air-exposed sediment	3
k_h	10^{-5}	m	water-height limitation constant	3

Table S3: List of model parameters. Continues from the previous page.

Affinity concentrations				
$k_{aeromin}$	10^{-5}	$mol\,O_2/m^3_{liquid}$	O_2 affinity of aerobic mineralization	1^c
k_{reox}	10^{-5}	$mol\,O_2/m^3_{liquid}$	O_2 affinity of ODU reoxidation	1^c
$k_{basalresp}$	10^{-5}	$mol\,O_2/m^3_{liquid}$	O_2 affinity of MPB basal respiration	1^c
Temperature Dependence				
$T_{photosyn,max}$	43.3	°C	Upper temperature boundary of MPB photosynthesis	3
$T_{photosyn,min}$	−30	°C	Lower temperature boundary of MPB photosynthesis	3
$T_{photosyn,opt}$	35.33	°C	Optimal temperature of MPB photosynthesis	3
$T_{reox,max}$	55	°C	Upper temperature boundary of ODU reoxidation	3
$T_{reox,min}$	−3.33	°C	Lower temperature boundary of ODU reoxidation	3
$T_{reox,opt}$	45	°C	Optimal temperature of ODU reoxidation	3
$T_{basalresp,max}$	48	°C	Upper temperature boundary of MPB basal respiration	3
$T_{basalresp,min}$	10	°C	Lower temperature boundary of MPB basal respiration	3
$T_{basalresp,opt}$	35	°C	Optimal temperature of MPB basal respiration	3

Source: (1) Parameters obtained from published literature, including [a]Brinkman et al. (2015), [b]Sanchez Zurano et al. (2021), [c]Nmor (2020); (2) Parameters measured directly or derived from observations; (3) Parameters derived by fitting model predictions to experimental data.

Table S4: List of model variables.

Name	Units	Description
Forcing variables		
T	°C	Ambient temperature
$I(0)$	µmol photons/m^2/s	Photosynthetically available radiation (PAR) at the sediment surface
h	m	Height of the overlying water column
Depth-dependent variables		
O_2	mol O_2/m$^3_{liquid}$	O_2 concentration (per liquid volume)
ODU	mol O_2/m$^3_{liquid}$	concentration of Oxygen Demand Units (per liquid volume)
I	µmol photons/m^2/s	Available light
C_{MPB}	mol C/m^3	MPB biomass (per bulk volume)
$R_{photosyn}$	mol O_2/m$^3_{liquid}$/d	O_2 production rate by MPB photosynthesis (per liquid volume)
$R_{aeromin}$	mol O_2/m$^3_{liquid}$/d	O_2 consumption rate by aerobic mineralization (per liquid volume)
R_{reox}	mol O_2/m$^3_{liquid}$/d	O_2 consumption rate by ODU reoxidation (per liquid volume)
$R_{basalresp}$	mol O_2/m$^3_{liquid}$/d	O_2 consumption rate by basal respiration (per liquid volume)
$R_{photoresp}$	mol O_2/m$^3_{liquid}$/d	O_2 consumption rate by photorespiration (per liquid volume)
$R_{consumption}$	mol O_2/m$^3_{liquid}$/d	total O_2 consumption rate (per liquid volume)
Fluxes and depth-integrated rates		
$J^{SWI}_{O_2}$	mol O_2/m^2/d	O_2 flux at the SWI
$J^{deep}_{O_2}$	mol O_2/m^2/d	O_2 flux at the lower boundary
J^{SWI}_{ODU}	mol O_2/m^2/d	ODU flux at the SWI
J^{deep}_{ODU}	mol O_2/m^2/d	ODU flux at the lower boundary
$J_{photosyn}$	mol O_2/m^2/d	Depth-integrated rate of photosynthesis
$J_{aeromin}$	mol O_2/m^2/d	Depth-integrated rate of aerobic mineralization
J_{reox}	mol O_2/m^2/d	Depth-integrated rate of ODU reoxidation
$J_{basalresp}$	mol O_2/m^2/d	Depth-integrated rate of basal respiration
$J_{photoresp}$	mol O_2/m^2/d	Depth-integrated rate of photorespiration
$J_{consumption}$	mol O_2/m^2/d	Depth-integrated rate of total O_2 consumption

Supplementary Figures

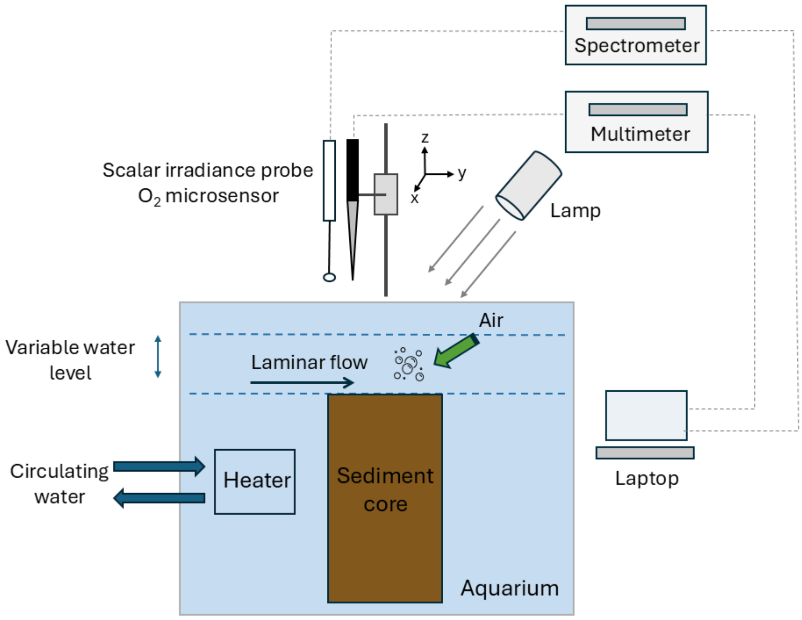

Figure S1: Schematic diagram of the experimental setup used in the present study. For further details, see Supplementary Methods, section "Technical details of the experimental setup".

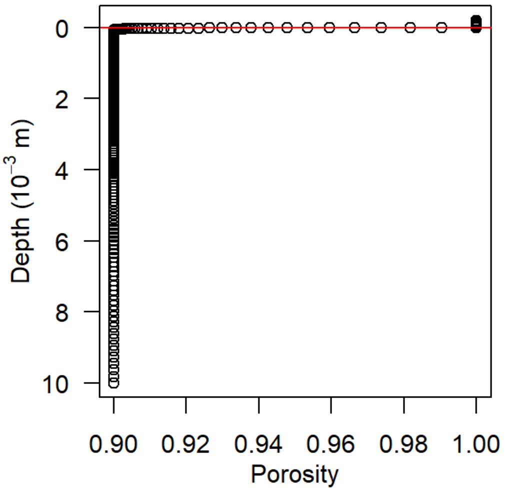

Figure S2: Porosity distribution along the modeled domain. Note the sharp decrease in porosity from 1 in the overlying water column to 0.9 just below the sediment surface.

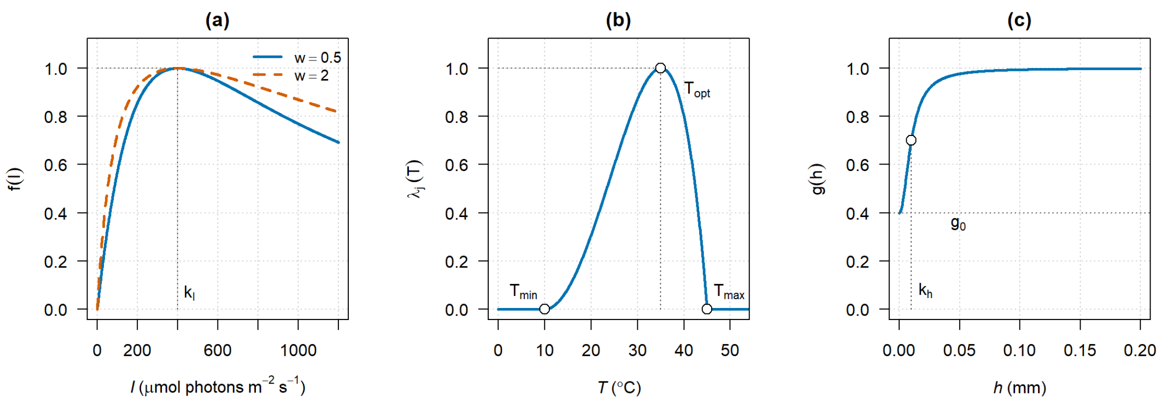

Figure S3: Illustration of the normalized response functions used in the model. (a) Light-response function of MPB photosynthesis (Eq. 6), illustrating the effect of the shape parameter w while keeping the optimum light intensity (k_I) constant. (b) Cardinal temperature-response function (Eq. 14), illustrating the three cardinal temperatures ($T_{\min}$, T_{opt}, and $T_{\max}$). (c) Water-height response function of MPB photosynthesis (Eq. 8), illustrating the reduction factor under dry conditions (g_0).

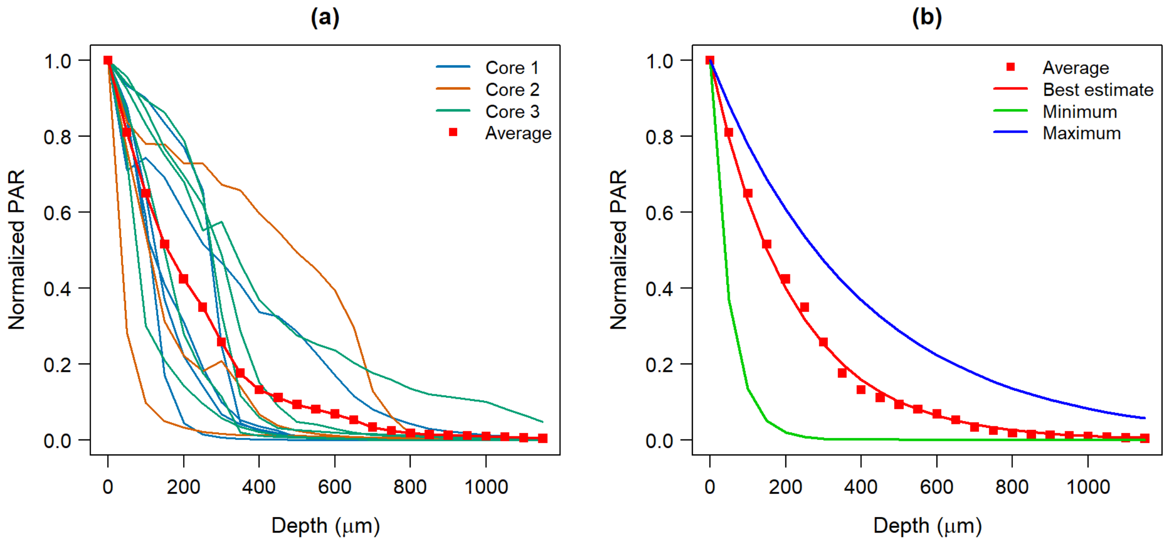

Figure S4: Light attenuation in the studied sediment. (a) Vertical profiles of scalar irradiance measured at different horizontal locations of three replicate sediment cores (see legend). Each profile is normalized to the maximum value reached at the SWI. Symbols show the (arithmetic) average. Differences between the profiles illustrate the degree of horizontal variability in light attenuation in the studied sediment. (b) Vertical profiles of light predicted by an exponential model (Eq. 7). Symbols show the same average profile as in panel (a), lines show the best estimate (red) and a realistic minimum (green) and maximum (blue), calculated with the k_{ext} values of 4.6 mm^{-1} (red), 20 mm^{-1} (green), and 2.5 mm^{-1} (blue). By defining the characteristic light penetration depth as a depth in the sediment where the light intensity decreases to 1 %of the value at the SWI (i.e., $\exp(-k_{ext} \cdot z_{light}) = 0.01$), these k_{ext} values translate to z_{light} of 1 mm, 0.23 mm, and 1.84 mm, respectively. Note that while some of the measured profiles deviate from the assumed exponential model, the average profile follows the exponential model reasonably well.

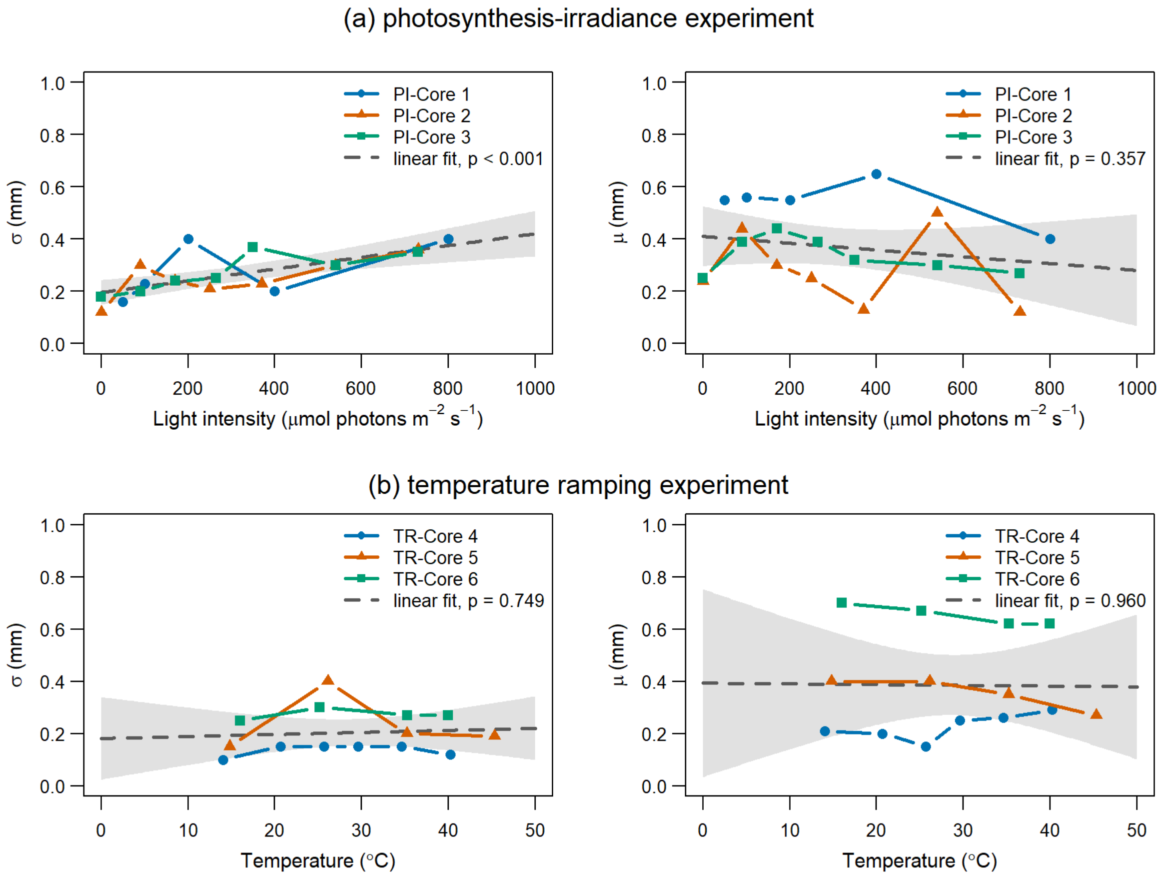

Figure S5: Response of the MPB biomass distribution to variations in incident light intensity (a) and temperature (b). Shown is the response of the parameters characterizing the spatial dispersion (σ, left column) and the position of the MPB biomass maximum (μ, right column). The parameter values were constrained based on the experimental data acquired in three replicate cores (see legend). The increasing trend of σ versus the incident light intensity (panel a) is significant ($p = 0.00095$; see Eq. 15 for the corresponding linear relationship), while the trends of μ versus light intensity ($p = 0.357$), σ versus temperature ($p = 0.749$), and μ versus temper-ature ($p = 0.960$) are not significant, as derived from a linear regression analysis.